Title

Surface Glycans Regulate Salmonella Infection-Dependent Directional Switch in Macrophage Galvanotaxis Independent of NanH

Journal

Infection and Immunity, 90(1)

ISSN

0019-9567

Authors

Sun, YH
Luxardi, G
Xu, G
et al.

Publication Date

2022-01-25

DOI

10.1128/iai.00516-21

Peer reviewed

AMERICAN SOCIETY FOR MICROBIOLOGY | Infection and Immunity®

CELLULAR MICROBIOLOGY:
PATHOGEN-HOST CELL MOLECULAR INTERACTIONS

Surface Glycans Regulate *Salmonella* Infection-Dependent Directional Switch in Macrophage Galvanotaxis Independent of NanH

Y. H. Sun,[a,b] G. Luxardi,[a] G. Xu,[c] K. Zhu,[a] B. Reid,[a] B. P. Guo,[d] C. B. Lebrilla,[c] E. Maverakis,[a] M. Zhao[a,e]

[a]Department of Dermatology, School of Medicine, University of California, Sacramento, California, USA
[b]Department of Internal Medicine, School of Medicine, University of California, Sacramento, California, USA
[c]Department of Chemistry, University of California, Davis, California, USA
[d]Office of Research, School of Medicine, University of California, Davis, Sacramento, California, USA
[e]Department of Ophthalmology, School of Medicine, University of California, Sacramento, California, USA

ABSTRACT *Salmonella* invades and disrupts gut epithelium integrity, creating an infection-generated electric field that can drive directional migration of macrophages, a process called galvanotaxis. Phagocytosis of bacteria reverses the direction of macrophage galvanotaxis, implicating a bioelectrical mechanism to initiate life-threatening disseminations. The force that drives direction reversal of macrophage galvanotaxis is not understood. One hypothesis is that *Salmonella* can alter the electrical properties of the macrophages by modifying host cell surface glycan composition, which is supported by the fact that cleavage of surface-exposed sialic acids with a bacterial neuraminidase severely impairs macrophage galvanotaxis, as well as phagocytosis. Here, we utilize N-glycan profiling by nanoLC-chip QTOF mass cytometry to characterize the bacterial neuraminidase-associated compositional shift of the macrophage glycocalyx, which revealed a decrease in sialylated and an increase in fucosylated and high mannose structures. The *Salmonella nanH* gene, encoding a putative neuraminidase, is required for invasion and internalization in a human colonic epithelial cell infection model. To determine whether NanH is required for the *Salmonella* infection-dependent direction reversal, we constructed and characterized a *nanH* deletion mutant and found that NanH is partially required for *Salmonella* infection in primary murine macrophages. However, compared to wild type *Salmonella*, infection with the *nanH* mutant only marginally reduced the cathode-oriented macrophage galvonotaxis, without canceling direction reversal. Together, these findings strongly suggest that while neuraminidase-mediated N-glycan modification impaired both macrophage phagocytosis and galvanotaxis, yet to be defined mechanisms other than NanH may play a more important role in bioelectrical control of macrophage trafficking, which potentially triggers dissemination.

KEYWORDS galvanotaxis, glycan, infection, macrophages, salmonella

Salmonella enterica is a common bacterial species that causes human diseases ranging from gastroenteritis to systemic infections. *Salmonella* spp. invade gut epithelia, preferentially by targeting the relatively small number of M cells located in the follicle-associated epithelium (1–3). Damage to enterocytes releases chemoattractive substances that attract immune cells such as neutrophils and macrophages —a process known as chemotaxis (4–7). Subsequent phagocytosis and clearance of the pathogens by immune cells usually stops the infection, resulting in no or mild symptoms. However, *Salmonella* has developed strategies, such as its type III secretion systems (8–12), to evade macrophage killing and survive inside the macrophage (13–16). Survival within the macrophage allows the pathogen to escape from its

Editor Manuela Raffatellu, University of California San Diego School of Medicine

Address correspondence to Y. H. Sun, yhsun@ucdavis.edu, or M. Zhao, minzhao@ucdavis.edu.

Received 14 September 2021
Accepted 4 October 2021
Accepted manuscript posted online 18 October 2021
Published 25 January 2022

entry site as soon as it reaches the bloodstream and spread systemically, resulting in life-threatening consequences (17–19).

Bioelectric signals have been implicated in development (20–23), wound healing (24–26), and regeneration (27, 28). In our initial study investigating the bioelectrical activities that contribute to active bacterial infections, we detected a *Salmonella* infection-generated electric field (IGEF) at the gut epithelium that drives anodal directional migration of primary murine macrophages *in vitro* (galvanotaxis: electric field-directed cell migration [21]). Such directional migration of macrophage galvanotaxis can be further reversed to the cathode upon *Salmonella* infection, implicating an alternative mechanism, other than chemotaxis, by which macrophages harboring live *Salmonella* egress from the original infection sites to initiate disseminated infections (29). The molecular elements that drive this *Salmonella* infection-dependent direction reversal in macrophage galvanotaxis, however, are not known. One hypothesis is that *Salmonella* can change the electrical properties of the macrophages by modifying host cell surface glycan composition, since cleavage of surface-exposed sialic acids with a bacterial neuraminidase leads to severely defective macrophage galvanotaxis. The *nanH* gene in *Salmonella enterica* subsp. *enterica serovar Typhimurium LT2* (KEGG ID: stm:STM0928) encodes a putative neuraminidase with specificity to NeuAc (30). The critical role of NanH for *Salmonella* invasion has been identified recently by demonstrating the importance of glycan desialylation during epithelial penetration, which is independent of the SPI-1 type III secretion system (31). We conducted glycomic analysis of macrophages and loss-of-function assessment of a *nanH* mutant in macrophage galvanotaxis to test this hypothesis.

RESULTS

Neuraminidase impairs macrophage galvanotaxis. Previously, we developed a mouse cecum model and detected a *Salmonella* infection-generated electric field (IGEF) at the gut epithelium. When applied *in vitro*, IGEF drove macrophage galvanotaxis to the anode, which was reversed to the cathode upon *Salmonella* infection (29). We confirmed that treatment with a potent bacterial neuraminidase significantly reduced macrophage surface negativities and severely impaired macrophage galvanotaxis (29) (Fig. 1A and B), resulting in 83% of the macrophages losing their polarity and 5% reversing polarity to the cathode (Fig. 1C). In contrast, the majority of the mock-treated control macrophages were polarized to the anode (86%) with a distinct morphology characterized by a leading pseudopodium of a dense actin meshwork and a rearward uropod (Fig. 1A and C).

Neuraminidase impairs macrophage phagocytosis. To learn if the neuraminidase treatment affects macrophage phagocytotic capacity, we challenged the macrophages with fluorescently labeled microspheres (1 μm, a similar size to *Salmonella*) before and after incubation with neuraminidase. We confirmed the potency of the reconstituted neuraminidase by assessing reduction in surface sialylated glycans by immunofluorescence labeling with *Maackia amurensis* lectin II (MAL-2, specifically binds to sialic acid in an α-2,3 linkage) (Fig. 1A and B), consistent with the role of this neuraminidase (32). We then quantified the number of cells containing beads and found that treatment with neuraminidase significantly ($P < 0.01$ by χ^2 test) reduced macrophage phagocytosis (mean percentages: 3.02, treated *versus* 19.83, not treated) (Fig. 1D). Together, these data suggest that the negatively charged surface glycans are not only critical for the electric field-guided directional migration but also important for their functional phagocytotic activities.

Neuraminidase modifies glycans on macrophages. The effect of neuraminidase on macrophage glycosylation can be readily characterized by global profiling of released host glycans. To establish the definitive role of the sialic acid cleaving enzyme, we conducted a comprehensive and quantitative N-glycan analysis of the neuraminidase treated macrophages, using high-resolution nanoLC-MS-based analytical tools capable of isomeric-level differentiation. The time points were chosen based on our previous experiments. They correspond to the time required for *Salmonella* to invade and establish intracellular growth in macrophages (29). Thus, in the subsequent discussions below, control and treated states refer to 0- and 30-min post-incubation, respectively.

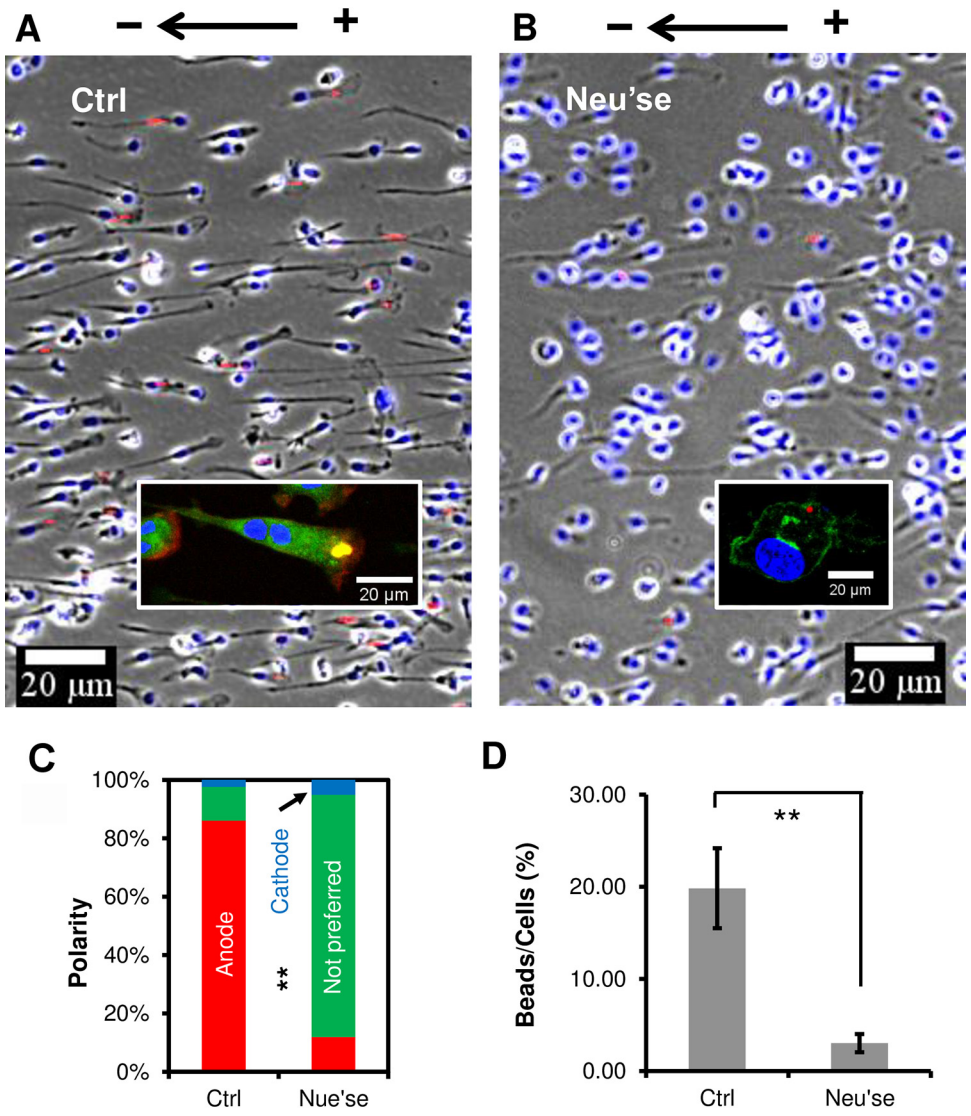

FIG 1 Neuraminidase impairs macrophage galvanotaxis and phagocytosis. (A) Screen shot of macrophages (Ctrl) challenged with 1-μm, red fluorescent microspheres, followed by 3-h exposure to an EF of 4 V cm^{-1} in the indicated orientation. Confocal image insert shows a macrophage containing a bead (pseudo-colored in yellow) was polarized to the anode. Sialylated glycans were labeled with Alexa 488-conjugated *Maackia amurensis* lectin II (MAL-2, in green). Actins were labeled with Alexa 546-conjugated phalloidin (red). Nuclei were counterstained with Hoechst 34222 (blue). Bar, 20 μm. (B) Screen shot of macrophages after neuraminidase treatment (Neu'se) challenged with 1-μm, red fluorescent microspheres, followed by 3-h exposure to an EF of 4 V cm^{-1} in the indicated orientation. Confocal image insert shows an unpolarized macrophage containing a bead. Sialylated glycans were labeled with Alexa 488-conjugated MAL-2 (green). Nuclei were counterstained with Hoechst 34222 (blue). Bar, 20 μm. (C) Polarity of macrophages treated with or without neuraminidase, followed by 3-h exposure to an EF of 4 V cm^{-1} in the indicated orientation. Data were quantified from a representative of three independent experiments. **, $P < 0.01$ by χ^2 test. (D) Quantification of phagocytosis of the macrophages with or without neuraminidase treatment. Data are presented as percentage of macrophages with beads (Mean $\pm$ SD) from three independent experiments. **, $P < 0.01$ by χ^2 test.

Individual N-glycans were identified by matching their molecular features, including accurate masses, isotope distributions, and retention times with a compositional library. Fig. 2A shows the abundances of different glycan types relative to the summed abundances of all glycans identified in the untreated and treated macrophages. Complex and hybrid type glycans were grouped together and then divided into different subgroups based on their levels of decoration (i.e., extension of the oligosaccharide chain by fucose, sialic acid, both, or neither), while high mannose glycans were grouped as a separate glycan type. Compared to untreated control, the neuraminidase-treated macrophages showed a decrease

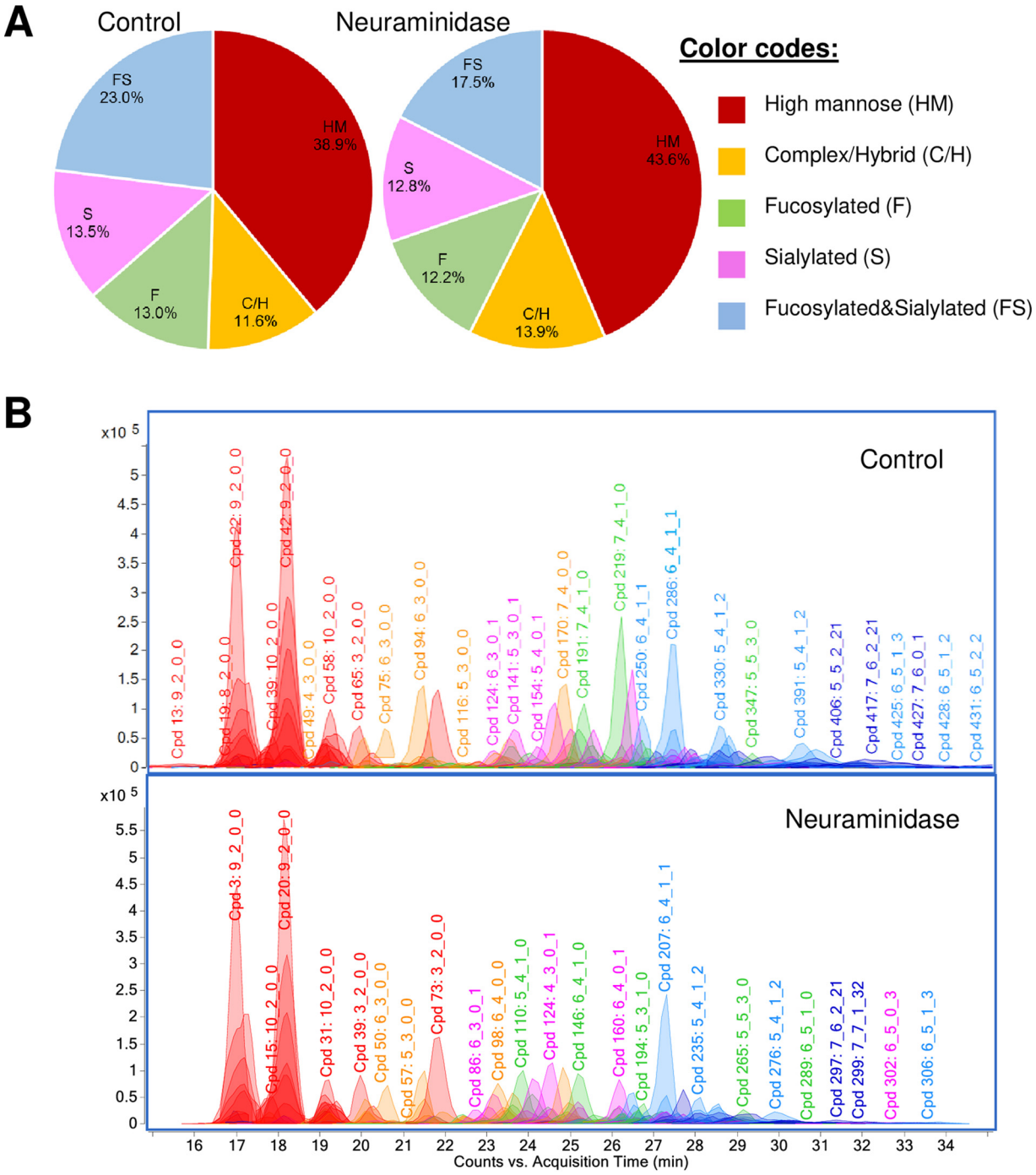

FIG 2 Neuraminidase reduces sialyation of surface-exposed N-glycans on macrophages. (A) Global compositional profiling of surface-exposed N-glycans on macrophages treated with neuraminidase versus untreated control cells. Pie charts show the summed abundances of surface-exposed N-glycans. (B) Comparison by number of sialic acids. (FS – #Sia: fucosylated & sialylated with 1–4 sialic acids). Data from a representative of two independent experiments, which produced similar results.

in sialylated glycans. Specifically, N-glycans that were both fucosylated and sialylated (FS) decreased by 6.5% from 23% in the control to 17.5% in the treated cells. The sialylated-only species (S) also had a decrease of 0.7% after treatment. Meanwhile, the summed relative abundance of non-sialylated and non-fucosylated species (C/H) increased by 2.3% from 11.6% to 13.9%, and the relative abundance of high mannose type glycans increased by 4.7% from 38.9% to 43.6% after treatment. Changes in sialylated species are particularly noteworthy given the predicted role of this enzyme (32). The concurrent decrease of sialylated structures

TABLE 1 Plasmids and *Salmonella* strains used in this study

	Description and Antibiotic Resistance	Reference or Source
Plasmids		
pKD119	Arabinose inducible λ Red recombinase expression plasmid. Temp sensitive. TetR	CGSC#: 7990
pKD4	Kan template plasmid for gene disruption. The resistance gene is flanked by FRT sites. AmpR, KanR.	(33) CGSC#: 7632
Salmonella		
IR715	ATCC 14028, NalR derivative	(69)
Δ*invA*	IR715 derivative, *invA*::Tn*phoA*, pGFT/RalFc, KanR, CmR	(29, 70)
LT2	*S. typhimurium* LT2	(69, 71)
Δ*nanH*	LT2 derivative, Δ*nanH*::Kan, KanR	This work

and increase of asialylated glycans is consistent with enzymatic degradation. We further note that desialylation appears to occur primarily on species that are both fucosylated and sialylated, given that afucosylated glycans bearing only sialic acid showed only a small decrease in their summed relative abundance and no significant changes in absolute abundances and in the number of compositions post-incubation. To examine the decreases in abundances of fucosylated and sialylated glycans in more detail, the degrees of fucosylation and sialylation in control and treated macrophages are compared in Fig. 2B. Mono- and difucosylated as well as mono- and disialylated structures represent the majority of decorated glycans on the macrophage surface prior to treatment. After incubation, decreases were observed such that asialylated structures became the most abundant. Of note, disialylated and trisialylated glycans showed the greatest decrease in their relative abundances by 4.8% from 8.4% to 3.6%, and 0.7% from 1.2% to 0.5%, respectively.

Construction of a *nanH* deletion mutant. STM0928 (30) in *Salmonella enterica* subsp. *enterica serovar Typhimurium LT2* (KEGG ID: stm:STM0928) encodes a putative neuraminidase gene named *nanH* that has the highest sequence identity (0.288 identical, data not shown) to the enzyme (KEGG ID: cpf:CPF_0721) we used in our macrophage treatment. The role of NanH for *Salmonella* invasion has only been realized recently by demonstrating the importance of glycan desialylation during epithelial penetration, which is independent of the SPI-1 type III secretion system (31). However, its role has not been investigated in macrophages. To assess the role of NanH in macrophage infection and to determine if NanH is required for the *Salmonella*-infection dependent directional switch in macrophage galvanotaxis, we constructed a Δ*nanH* mutant in *Salmonella* LT2 using the λ Red recombination engineering system as described previously (33), which involves a simple one-step strategy. We used plasmid pKD4 as a template to generate PCR products of the Kan-resistant gene flanked by 50-bp sequence homologous to *nanH* (Fig. S1A). We then electroporated the purified PCR products into competent *Salmonella* LT2 containing temperature-sensitive and tetracycline-resistant pKD119. Expression of λ Red recombinase at low temperature (30°C) and induced by addition of L-arabinose promotes recombination of the Kan element into the chromosome between the *nanH* homologous sequences. Recombinants were selected for kanamycin resistance and cured with a high-temperature shock (40°C for 30 min) followed by culture at physiological temperature (37°C). We screened for loss of temperature-sensitive pKD119 by selecting for sensitivity to tetracycline. The deletion of *nanH* was confirmed by PCR (Fig. S1B) and by Sanger sequencing (Fig. S1C). The strains and plasmids constructed in this work are listed in Table 1.

NanH is required for *Salmonella* infection in primary murine macrophages. A recent study showed that deletion of *nanH* significantly decreases invasion in polarized colon epithelial cells, suggesting its important role during *Salmonella* infection (31). To determine specifically whether NanH is required for resistance of macrophage killing, we assayed the ability of the *nanH* mutant to survive in bone marrow-derived murine macrophages (BMDM). For these experiments, we challenged macrophages with both the *nanH* mutant and its parental wild type stain (LT2) at an MOI of 20 (20 bacteria per cell) and a low MOI of 5. Deletion of *nanH* decreased the ability of *Salmonella* to survive within macrophages at 16 h after infection, resulting in an approximately 4-fold decrease in recovery of the mutant compared to of the wild type. The difference between the mutant and wild type was statistically significant ($P < 0.05$) at the MOI of 5 (Fig. 3A). To further

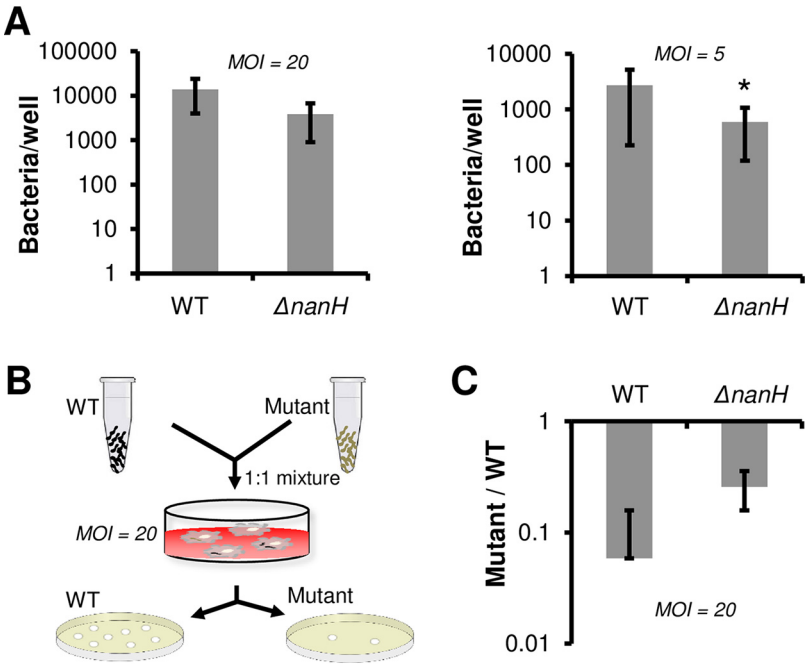

FIG 3 Recovery of *nanH* mutant after infection of macrophages. (A) Inocula of the *nanH* mutant and the wild type (WT) was used to challenge bone marrow-derived macrophages (BMDMs) separately. Intracellular bacteria were recovered after 16 h as described in Materials and Methods. *, $P < 0.05$ by unpaired Student's *t* test. (B) Schematic of the competitive of competitive assay. (C) Mixed inocula of the *invA* or *nanH* mutant and their respective wild type were used to challenge BMDMs at MOI of 20. Intracellular bacteria were recovered after 16 h as described in Materials and Methods. Competitive index (C.I.), calculated as log (CFU mutant/CFU wild type), is shown on the *y* axis. Data shown are the means of three independent assays done in triplicate with standard deviations shown.

verify the observed attenuated phenotype, we performed a competitive index assay of the *nanH* mutant against its wild-type strain, as coinfection provides a sensitive measure of differences between the wild type and the mutant with respect to intracellular survival (34, 35) (Fig. 3B). Inocula containing 1:1 mixtures of wild type and Δ*nanH* were used to infect BMDM cultures at an MOI of 20. In parallel, coinfection of Δ*invA* and its wild-type strain (IR715) showed that at 16 h after infection, the CFU of Δ*invA* recovered was 1/20 that of IR715, demonstrating that under these conditions the wild type is not able to rescue a mutant lacking a functional SPI-1 T3SS, and validating the efficacy of the competitive assay in our primary murine macrophage infection setup. Importantly, the competitive index of *nanH* mutant *versus* wild type recovered from BMDMs was 1/4 (Fig. 3C). Based on these results, we concluded that NanH is required, but not essential (relevant to Δ*invA*), for the infection of primary murine macrophages.

The *nanH* mutant reduces cathode migration in macrophage galvanotaxis without canceling infection-dependent direction reversal. Previously, we demonstrated that *Salmonella* infection can reverse macrophage galvanotaxis *in vitro*, implicating an initial mechanism, other than chemotaxis, of disseminating infections (29). In view of the phenotypic potential of *nanH* as a candidate virulence factor to establish intracellular growth in macrophages, we investigated its role in contributing to the infection-dependent direction reversal in macrophage galvanotaxis. We infected BMDMs with WT *Salmonella* or *nanH* mutant and monitored their migratory behaviors in response to an applied EF. First, we conducted macrophage galvanotaxis assays at 30 min postinfection since this was the time (Fig. 1) at which we initially observed galvanotactic defects in macrophages incubated with neuraminidase. While 92% control macrophages underwent directional migration to the anode (mean directedness of 0.76), only 65% of macrophages challenged with WT *Salmonella* and 75% of macrophages challenged with *nanH* mutant migrated to the anode (Fig. S2A and B), resulting in a significantly reduced mean directness of 0.47 and 0.21, respectively (Fig. S2C).

Although the overall reductions in directedness between WT- and *nanH* mutant-challenged macrophages is not significant, these data suggest that with a such short period of challenge time, *Salmonella* infection is taking an action to affect macrophage galvanotaxis. At this early time point, the migration speeds of the macrophages challenged with either WT *Salmonella* or *nanH* mutant in response to applied EF were not significantly affected (Fig. S2D).

Since challenging *Salmonella* did not reverse macrophage directional migration in response to applied EFs, our subsequent experiments were carried out at 16 h postinfection. As controls, macrophages challenged with fluorescently labeled microspheres of similar size to bacteria were also included and monitored under identical conditions (Fig. 4A).

While 96% to 97% macrophages challenged with or without beads underwent unidirectional migration to the anode (mean directedness of −0.91 and −0.90, respectively), 66% of macrophages infected with WT *Salmonella* reversed their directional migration to the cathode, resulting in a mean directness of 0.35. These data, as highlighted by the trajectories and polarization plots (Fig. 4B and C), are consistent with our previous observations (29), suggesting that the direction switch was not caused by phagocytosis *per se* (i.e., the phagocytosis of beads), but was *Salmonella* infection dependent. In contrast, macrophages challenged with the *nanH* mutant reduced direction reversal compared to those challenged with WT *Salmonella*, resulting in a mean directness of −0.11. Such reduction in directionality, however, was not restored back to the control level, nor to that of the macrophages challenged with microspheres (Fig. 4D). We also quantified migration velocities of macrophages in response to applied EFs under different challenge conditions but identical experimental settings. We were unable to detect significant differences in migration speed between any groups, either WT *versus nanH* mutant, or the groups challenged with *Salmonella versus* groups not challenged or challenged with microspheres (Fig. 4E). However, comparison and statistical analysis of displacement speed (defined by Euclidean distance of cell migration divided by time) revealed that macrophages challenged with live *Salmonella* were significantly slower than cells not challenged or challenged with microspheres (Fig. S3), suggesting that *Salmonella* infection may affect the directional migration efficacy of macrophages in response to EFs.

***Salmonella* mutants lacking *nanH* reduce surface-exposed sialic acids in macrophages at wild-type level.** Since challenging macrophages with *nanH* mutants only marginally affected direction reversal, we then looked at the zeta potential of the macrophages infected with Δ*nanH*. While the negativities of surface-exposed glycans were indeed reduced (less negative), the reduction in macrophages resulting from Δ*nanH* infection was insignificant, compared to that caused by WT *Salmonella* infection (Fig. 5A). Accordingly, the surface-exposed sialic acids—a major contributor of the negative zeta potential, which was previously reported to be reduced by *Salmonella* infection (29), were similar between the macrophages challenged with WT or Δ*nanH*, as demonstrated by flow cytometry with MAL-2 labeling (Fig. 5B). Together, these data strongly suggest the existence of other major factor(s), besides NanH, involved in the reduction of macrophage surface negativity contributing to *Salmonella* infection-dependent direction switch in macrophage galvanotaxis.

DISCUSSION

Negative electric charges on the macrophage surface is one of the most critical factors responsible for microorganism and particle attachment to initiate phagocytosis (36), presumably through the binding of surface-exposed glycosylated ligands (37). It has been proposed that modulation of surface charges could alter the phagocytic function of macrophages. For example, treatment with *Vibrio cholerae* neuraminidase promotes the attachment of pathogenic *E. coli* to and phagocytosis by peritoneal macrophages *in vitro* and *in vivo* (38). Previously, we reported that treatment with a potent bacterial neuraminidase significantly reduces macrophage surface negativities and severely impaired macrophage galvanotaxis (29). Here, we performed functional studies, which demonstrated that neuraminidase-induced macrophage glycocalyx compositional changes reduced cell surface electric

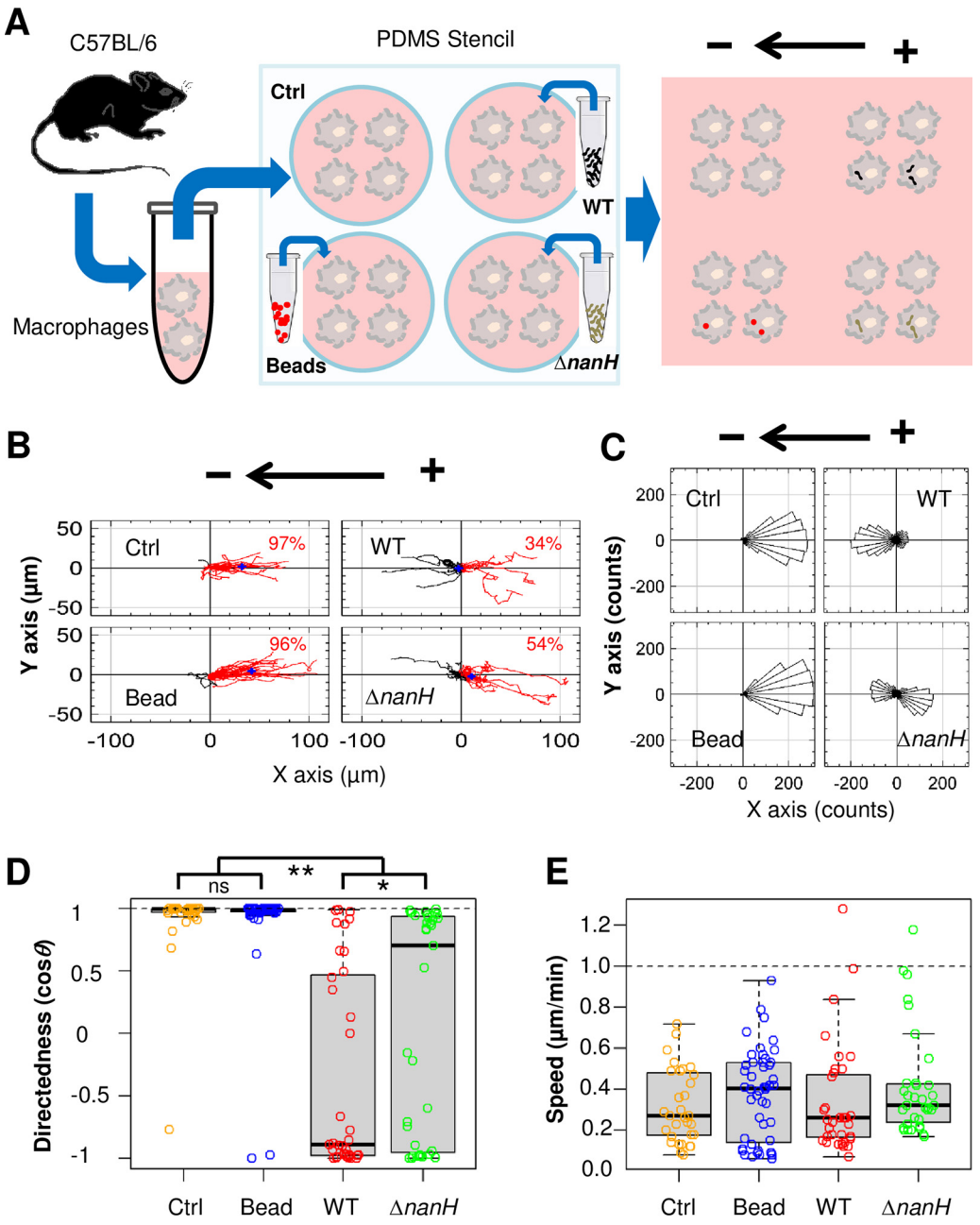

FIG 4 Infection with *nanH* mutant reduced *Salmonella*-infection dependent direction reversal in macrophage galvanotaxis. (A) Schematic of the experimental design. Freshly differentiated mouse BMDMs from C57B/6 mice were seeded in wells engineered with a PDMS stencil. Adhered macrophages were challenged with either red fluorescent beads ("Bead") or WT *Salmonella* (WT) or *nanH* mutant (Δ*nanH*) and cultured for 16 h. Unchallenged BMDMs served as the control (Ctrl). Subsequent migration of macrophages was monitored in the same galvanotaxis chamber under identical conditions after removal of the PDMS stencil, as described in Materials and Methods. (B) Trajectories (red: to the anode, numbers indicating percentage of cells migrated to the anode; black: to the cathode; blue crosses: centroid) and (C) polarization graphs of Ctrl macrophages or macrophages challenged with beads or WT *Salmonella* or Δ*nanH* mutant exposed to an EF of 4 V cm^{-1} for 3 h in the indicated orientation. (D) Box-and-Whisker plot of directedness and (E) migration speed (see also Movie 1) of macrophages under different challenge conditions. *, $P < 0.05$ or **, $P < 0.01$ by one-way ANOVA with *post hoc* Tukey HSD test, ns: nonsignificant.

negativity and dramatically affected macrophage phagocytotic function as evidenced by decreased phagocytosis of microspheres (Fig. 1). Given that phagocytosis (of the microspheres) *per se* did not cause dramatic changes in surface glycans and/or negativity of the macrophage (29), our data suggest that macrophages take up this type of microsphere

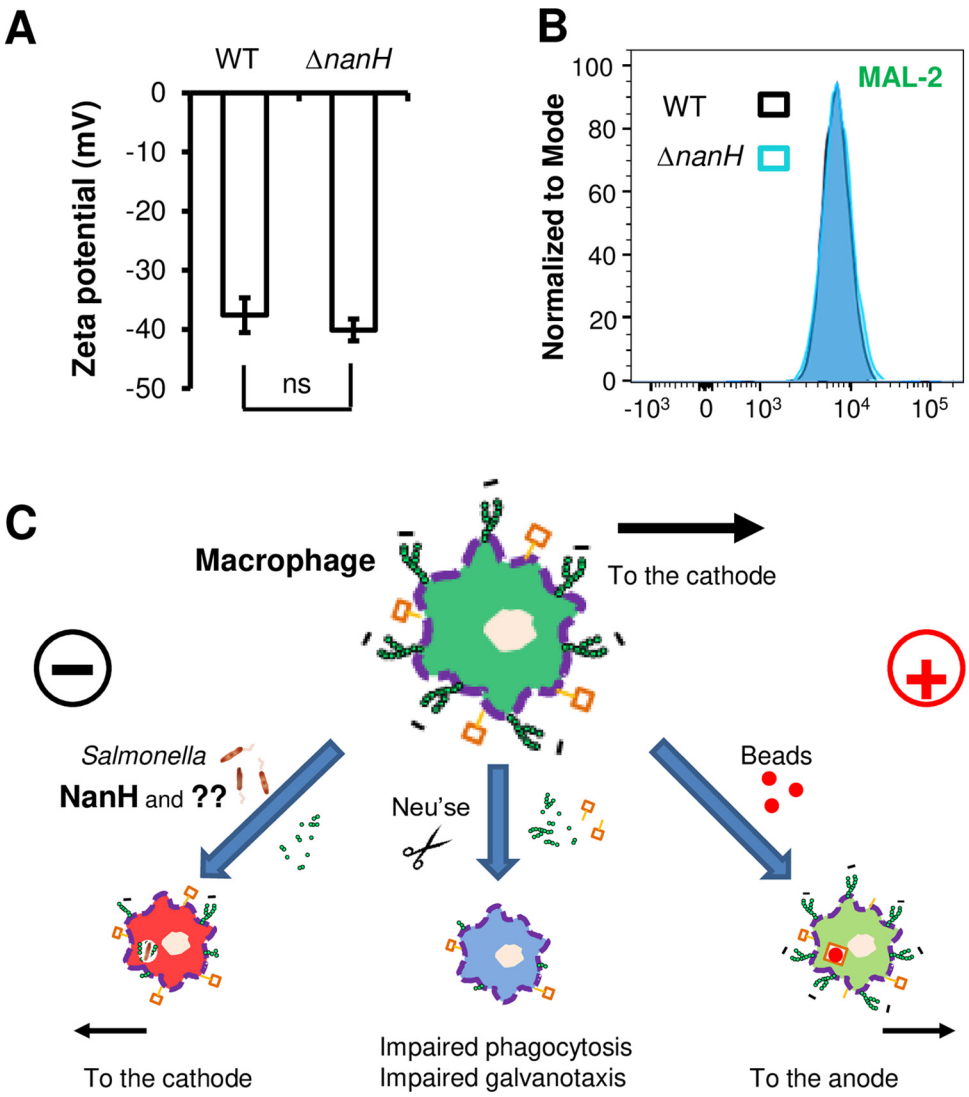

FIG 5 NanH and yet-to-be-identified factor(s) contribute to *Salmonella* infection-dependent direction switch in macrophage galvanotaxis. (A) Zeta potentials or (B) Representative flow cytograms of standardized MAL-2 fluorescence intensity of macrophages infected by wild type *Salmonella* (WT) or Δ*nanH*. ns, nonsignificant by Student's *t* test. (C) Model of *Salmonella* infection-dependent direction switch in macrophage galvanotaxis through neuraminidase-mediated glycan modifications. Negatively charged macrophages with terminally sialylated surface structures (small green circles) undergo robust directional migration to the anode. Phagocytosing *Salmonella* decreases sialic acid composition and subsequently reduces surface negativity of the macrophage through combined activities of NanH and other glycan dehydrases or other unknown effectors (question markers). Enzymatic cleavage of sialic acids (possibly other glycans as well) by incubation of neuraminidase (scissors) impairs macrophage galvanotaxis, as well as phagocytosis. Macrophages that phagocytosed beads through binding of non-sialylated surface components (brown squares) still migrate to the anode.

through a different route without significantly changing their electric negativities, thus, still migrating to the anode (Fig. 5C).

By integrating mass spectrometry and biochemical glycomic approaches, we generated detailed N-glycan structural profiles of the mouse primary macrophage, which we then used to identify glycan alterations that may have functional significance. The N-glycome of neuraminidase-treated macrophages (by incubation with a potent bacterial neuraminidase) differed from that of bone marrow-derived naive macrophages. Specifically, compared to naive macrophages, neuraminidase-treated macrophages had decreased sialylated N-glycans, including fewer fucosylated/sialylated complex N-glycans. Conversely, the relative abundance of non-sialylated species was increased after neuraminidase treatment (Fig. 2A). Unlike enzymatically treated macrophages, mono- or disialylated glycans were the dominant complex

structures on the untreated macrophage surface, which contribute negative charge to the cell membrane. This intrinsic bioelectrical property of macrophages may contribute to their robust galvanotactic responses such as directed migration to the anode (Fig. 1), which we and others have consistently demonstrated (29, 39). Following neuraminidase incubation, negatively charged N-glycans such as disialylated and trisialylated glycans were significantly reduced (Fig. 2B). This decrease is likely to affect directional migration of macrophages in response to electrical stimuli by increased zeta potentials (reduced surface negativity) (29, 40), and subsequently through bioelectrically and biochemically coupled signaling pathways (25, 41). Using a mouse typhoid model, we have demonstrated that *Salmonella* infection generates minute electric fields at the gut epithelium, which can drive directional migration of macrophages to the anode *in vitro*, presumably recruiting macrophages to an infection site. We also showed that infecting macrophages with *Salmonella* reduces macrophage surface zeta potential and reverses directional migration of macrophages to the cathode, presumably driving macrophages containing live bacteria away from an infection site to initiate systemic disseminations (29). Hence, comprehensive N-glycan profiling by nanoLC-chip QTOF mass cytometry employed in this study suggests a mechanistic feature of disseminated *Salmonella* infections. The results provide compelling evidence at the molecular level for the notion that modification of host glycan structures contributes to dissemination of *Salmonella*, suggesting that the pathogen manipulates directional migration behavior of the macrophage in part by modifying host surface glycan composition, specifically through desialylation. Moreover, the sialic acid cleavages provide evidence that the enzyme might be delivered during the pathogen-host interaction phase, an idea that has been proposed previously based on the enzyme's crystal structure (42). The present report is the first to identify a glycosyl hydrolase that affects macrophage galvanotaxis, besides the impairment of phagocytosis (Fig. 1). Given the nature of the cleavages, the putative neuraminidase encoded by STM0928 is likely responsible for the majority of host desialylation by *S. typhimurium* (30).

Bacterial neuraminidases have been considered virulence factors in many pathogenic bacteria such as *V. cholerae* and *Clostridium perfringens* (43, 44). The *nanH* gene in *S. enterica* serovar Typhimurium LT2 resides in a P2-like prophage (Fels-1) (45, 46) and encodes a putative neuraminidase (30). Unlike other bacterial neuraminidases, NanH of *Salmonella* is structurally close to *H. influenzae* viral sialidase as revealed by crystal structure studies (42, 47). *In vitro*, *Salmonella* NanH shows kinetic preference for sialyl α2-3 linkages over sialyl α2-6 linkages and preferentially cleaves Neu5Ac residues rather than N-glycolylneuraminic acid (Neu5Gc) residues (48). NanH is induced in the late growth phase, but its enzymatic activity is not increased greatly by free sialic acid (49). Collectively, studies on the genetics, structure, and biochemistry of *Salmonella* NanH reviewed above indicate a virulence, rather than metabolic role in *Salmonella* infection. However, the role of NanH in *Salmonella* virulence has not been revealed until recently by a study demonstrating that *Salmonella* requires NanH, as well as other keystone glycosidases, for invasion of colonic epithelial cells (31). Consistent with this observation, NanH is required in part for *Salmonella* infection in primary murine macrophages (Fig. 3). It remains unclear how *Salmonella* delivers the NanH. One possibility is through direct secretion or release into the culture environment, which is in line with the observation that enzymatic treatment for just 30 min *in vitro* is sufficient for the modification of macrophage surface glycans and zeta potentials, resulting in consequently phagocytic and galvanotactic impairments. This, however, is not conclusive as we were unable to detect galvanotactic differences between the macrophages infected by either WT or *nanH* mutant in just 30 min of incubation time (Fig. S3). It is well known that bacterial enzyme activities *in vitro* are more potent and kinetically faster under similar conditions *in vivo* due to optimized pleiotropic effects of ions and absence of complex inhibitory/regulatory networks (50). In the infection scenario, the short period of incubation time, including the time required for phagocytosing and processing bacterial pathogens is unlikely to be sufficient for the macrophages to switch direction since cells in response to applied EF, undergoing directional migration itself is a complex biological process and requires signal transduction, multiple intracellular signal cascades, and even gene transcription (21, 25). Another possibility is by injection/secretion through the SPI-2 system since most of virulence factors carried in

prophages in *Salmonella* are also SPI-2 effectors (45, 46, 51, 52). Further extensive work is needed to test this prediction. It also remains unclear if NanH is required for *Salmonella* infection *in vivo*. Surprisingly enough, previous work by lysogenic conversion of a *fels-1*-lacking *S. enterica* serovar Typhimurium strain with Fels-1 did not enhance mouse virulence (45). However, this does not exclude the possibility that NanH is required for long-term systemic infection, as is the case for the prophage-coded SPI-2 effector SseI (53). Future work using the model of long-term chronic *Salmonella* infection in mice (53) will shed light on this long-standing enigma.

It is important to note that while NanH-dependent macrophage glycocalyx modification reduced *Salmonella* infection-dependent direction switch, infection with the *nanH* mutant did not eliminate direction reversal entirely (Fig. 4), strongly suggesting that NanH alone is insufficient for the *Salmonella* infection-dependent direction reversal in macrophage galvanotaxis, and that other molecules/mechanisms, independent of NanH, must exist. For instance, *S. typhimurium* possesses at least 51 endogenous glycosyl hydrolases (some annotations remain putative) that likely function in glycan degradation (54). Although their roles underlying invasion of macrophages (as well as intestinal epithelial cells) remain unclear, we speculate that these enzymes collectively engage in the observed desialyation during *Salmonella*-macrophage interaction. Therefore, it is not surprising that infection with Δ*nanH* still leads to reduced surface negativity of macrophages at the wild type level, as supported by the zeta potential measurements (Fig. 5A). Moreover, macrophages express Toll-like receptors (TLRs) that recognize structurally conserved molecules derived from *Salmonella* and other pathogens. All TLRs contain *N*-linked glycosylation consensus sites and both TLR2 and TLR4 require glycosylation for surface translocation and function (55, 56). Interestingly, both α2-3- and α2-6-linked SAs on the cell surface decreased during macrophage differentiation and polarization, which was in accordance with the increase of the siaoglycoconjugates inside the cells (57), Binding of *Salmonella* to these glycosylated receptors and subsequent internalization may reduce surface negativity of macrophages, leading to directional switch under EF. The roles of *Salmonella* lipopolysaccharide (LPS, a potential TLR4 ligand) and lipoproteins in mediating macrophage migration and galvanotaxis in particular, warrant future work.

The picture emerging from this, and previous works is that desialytion of surface-exposed N-glycans of macrophages occurs during *Salmonella* infection, which reduces the negative electric charge on the host cell surface (34) (Fig. 5C). Modification of glycans and subsequent reduction of surface negativity allows macrophages harboring live *Salmonella* to switch migration direction in response to IGEF. This outcome is biologically relevant because escaping from the infected sites at the gut epithelium to reach lymphatic drainage and/or bloodstream is a critical initial step for *Salmonella* dissemination (17, 58).

MATERIALS AND METHODS

Isolation and culture of bone marrow-derived macrophages. The mouse strains used were in a C57BL/6 background (both male and female mice were used in experiments). Mice were purchased from Jackson labs and maintained under a strict 12-h light cycle and given a regular chow diet in a specific pathogen-free facility at University of California (UC), Davis. All animal experiments were performed in accordance with regulatory guidelines and standards set by the Institutional Animal Care and Use Committee of UC Davis. Bone marrow-derived macrophages (BMDMs) were isolated following standard procedures as previously described (59). BMDMs were cultured in DMEM (Invitrogen) with 10% Fetal Bovine Serum (Invitrogen) and 1× Antibiotic-Antimycotic solution (Invitrogen), supplemented with 20% L-929 conditioned medium for 6 days (plus an extra feed at day 3), followed by 1-day culture without the conditioned medium. Adherent macrophages were then harvested by gently scraping with a "policeman" cell scraper and used for subsequent experiments accordingly. Cell viability was determined by trypan blue staining and counting.

Construction of the *nanH* mutant in *Salmonella enterica subsp. enterica serovar Typhimurium LT2*. The *nanH* mutant was made using the λ Red recombination engineering strategy as described by Datsenko and Wanner (33). In brief, primers of NanHKan-F (5′-AGAAATAACGGTAATCATATGTTTGACCAGACAT CTACTTAACTGCAGAATACTGTGTAGGCTGGAGCTGCTTC-3′) and NanHKan-R (5′-AGCAGCAATGGCTATTTTTTGA TGTTTAATTGTATGATTTTATTACTGGTAAATTCCGGGGATCCGTCGACC −3′), and plasmid pKD4 as a template were used to generate PCR products of the Kan resistance gene flanked by 50-bp homologies of *nanH* (Fig. S1A). Purified products were electroporated into competent *Salmonella* LT2 containing temperature-sensitive pKD119. Expression of λ Red recombinase induced by addition of L-arabinose promotes recombination of the Kan element between the homologies. Recombinants were selected for kanamycin resistance and tetracycline sensitivity. The deletion of *nanH* was confirmed using PCR (Fig. S1B) with primers of NanH-F (5′-TCATATGTTTGACCAGAC

ATCTACTTAACTG-3′) and NanH-R (5′-GTCTAGATGTTTAATTGTATGATTTTATTACTG-3′), and by Sanger sequencing (Fig. S1C). The strains and plasmids constructed in this work are listed in Table 1.

Cell membrane extraction. Details of the isolation of the cell membrane fraction have been described previously (30, 31). In brief, harvested cells were resuspended in homogenization buffer containing 0.25 M sucrose, 20 mM HEPES-KOH (pH 7.4), and 1:100 protease inhibitor mixture (EMD Millipore, Billerica, MA). Cells were lysed on ice using a probe sonicator (Qsonica, Newtown, CT) and lysates were centrifuged at 2000 $\times$ *g* for 10 min to remove the nuclear fraction and debris. The supernatant was then resuspended and ultracentrifuged in a series of three different buffers at 200,000 $\times$ *g* for 45 min at 4°C to remove the endoplasmic reticulum and cytoplasmic fraction. The resulting membrane pellet was isolated and stored at −20°C until further processing.

N-Glycan release and enrichment. Membrane pellets were suspended with 100 μl of 100 mM ammonium bicarbonate in 5 mM dithiothreitol and heated for 10 s at 100°C to thermally denature the proteins. To release the glycans, 2 μl of peptide N-glycosidase F (PNGase F) (New England Biolabs, Ipswich, MA) was added to the samples and incubated at 37°C in a microwave reactor (CEM Corporation, Matthews, NC) for 10 min at 20 W. After addition of 400 μl of ice-cold ethanol, samples were frozen for 1 h at −80°C and centrifuged for 20 min at 21,000 $\times$ *g* to precipitate deglycosylated proteins.

Released N-glycans in the supernatant were purified by solid phase extraction (SPE)1 using porous graphitized carbon (PGC) cartridges (Grace, Chicago, IL). Cartridges were first equilibrated with alternating washes of nanopure water and a solution of 80% (vol/vol) acetonitrile and 0.05% (vol/vol) trifluoroacetic acid in water. Samples were loaded onto the cartridges and washed with nanopure water to remove salts and buffer. N-glycans were eluted with a solution of 40% (vol/vol) acetonitrile and 0.05% (vol/vol) trifluoroacetic acid in water and dried *in vacuo*.

N-glycan analysis by LC-MS/MS. The purified N-glycans were reconstituted in 30 μl of water, and 5 μl of each sample was injected to an Agilent nanoLC-chip-QTOF-MS system (Agilent Technologies, CA) for analysis. Samples were introduced into the MS with a microfluidic chip, which consists of enrichment and analytical columns packed with porous graphitized carbon and a nanoelectrospray tip. A binary gradient was applied to separate and elute glycans at a flow rate of 0.3 μl/min: (A) 3% (vol/vol) acetonitrile and 0.1% (vol/vol) formic acid in water and (B) 90% (vol/vol) acetonitrile in 1% (vol/vol) formic acid in water. MS spectra were acquired at 1.5 s per spectrum over a mass range of *m/z* 600–2000 in positive ionization mode. Mass inaccuracies were corrected with reference mass *m/z* 1221.991. Collision-induced dissociation (CID) was performed with nitrogen gas using a series of collision energies ($V_{collision}$) dependent on the *m/z* values of the N-glycans, based on the equation: $V_{collision}$ = *m/z* (1.8/100 Da) V −2.4 V. N-glycans from each data file were then identified and extracted by matching their accurate masses and isotope patterns with an in-house cell membrane N-glycan compositional library using the molecular feature finding function in MassHunter software (Agilent, CA).

Gentamycin protection assay to determine intracellular bacterial CFU. The gentamicin protection assays were carried out as previously described (60). In 24-well tissue culture-treated plates, 2 $\times$ 10^5 cells were seeded per well for 5–6 h in culture medium (DMEM with 10% Fetal Bovine Serum and no antibiotics). Wild type *Salmonella* or mutants were grown overnight and used to infect macrophages, either alone or in a mixture 1:1, at a multiplicity of infection (MOI) of 5 or 20. After 60 min of incubation, cells were gently washed 3$\times$ with PBS, and further incubated in gentamicin-containing culture media at a final concentration of 50 μg ml^{-1} for additional 60 min. Afterwards medium was replaced with culture media containing 10 μg ml^{-1} gentamicin for the duration of the experiment. Intracellular CFU was measured at 16 h PI. To measure intracellular CFU, macrophages were lysed using 0.5% Tween 20 for 5 min at room temperature and released by scraping with 1 ml pipette tips. CFU were enumerated by plating on LB agar with or without 100 μg/ml kanamycin. For the competitive assay, competitive index (C.I.) was calculated as log (CFU mutant/CFU wild type) (Fig. 3B).

Infection, challenge, and treatment of macrophages. Typically, 4 $\times$ 10^4 primary mouse macrophages were seeded per well of engineered silicon stencils sealed in custom-made electric field (EF) chambers (29) or 96-well glass bottom plates (Nunc), or 2 $\times$ 10^5 cells per well in 24-well tissue culture-treated plates or 1 $\times$ 10^6 cells per well in 6-well tissue culture-treated plates depending on different experiment needs, for 5–6 h in culture medium. Overnight cultures of *Salmonella* or 1.0 μm, red fluorescent (580/605) carboxylate-modified microspheres (Invitrogen) were used to infect/challenge macrophages at an MOI of 20. The rest of the procedures were similar to that of the gentamicin protection assay. Cells were cultured in medium containing 10 μg ml^{-1} gentamicin for 16 h and subsequent galvanotaxis experiments were carried out in the same medium containing gentamicin.

For the galvanotaxis assay at 30 min postinfection, cells were challenged for only 30 min and washed with medium containing 50 μg ml^{-1} gentamicin. Experiments were carried out in culture medium containing 10 μg ml^{-1} gentamicin.

For the neuraminidase treatment, cells were incubated in culture medium containing 100 mU ml^{-1} neuraminidase from *Vibrio cholerae* (Sigma-Aldrich) for 30 min at 37°C (40). Cells were then washed with culture medium, and either harvested or subjected to microsphere challenge. Subsequent galvanotaxis experiments were carried out in the culture medium containing no neuraminidase.

Galvanotaxis assay. *Engineering silicone stencil and EF chamber design.* We have tested cover glass and plastics coated with different substrates and found that macrophages perform robust and consistent galvanotaxis when cultured in tissue culture dishes (Corning). Therefore, our EF chambers were customized based on 100-mm tissue culture dishes. To facilitate group comparability and EF control, we engineered removable and reusable silicone stencils of multiple wells (diameter of 8 mm, thickness of 2.4 mm) to seed the same batch of cells that can be challenged/treated with different bacteria/substances and monitored under identical galvanotactic conditions simultaneously (61). The EF tunnel height is fixed at around 120 μm by double-sided silicone tapes cut by a computer-controlled laser cutter (62).

EF application and time-lapse recording. We applied exogenous EF as previously described (61, 63–65). The EF strength is based on the infection-generated EF (IGEF) we measured at the gut epithelium

(29). Actual EF strengths were measured and determined with a voltmeter before and after each EF application. Cell migration was monitored with a Carl Zeiss Observer Z1 inverted microscope equipped with a motorized stage and an incubation chamber (37°C and 5% CO_2). Time-lapse contrast images and/or images of appropriate RFP channel were captured using MetaMorph NX program (Molecular Devices). A Retiga R6 (QImaging) scientific CCD camera were used to detect and monitor macrophage movement. Typically, in each experiment, 2 to 4 fields of each condition under a 10× or a long-distance 20× lens were chosen. Images were taken at 5 min intervals for up to 3 h unless stated otherwise.

Image processing and data analysis/presentation. Time-lapse images were imported, processed, and assembled in ImageJ (http://rsbweb.nih.gov/ij). To quantify single-cell and population motility we extracted the trajectory of each cell migration (>30 cells for each condition) using an automatic/manual tracking tool (41, 61, 65). Directionality as directedness in cosine theta (θ), where θ is the angle that each cell moved with respect to the EF vector, were quantified from the coordinates of each trajectory (66, 67). If a cell moved perfectly along the field vector toward the cathode, the cosine of this angle would be 1; if the cell moved perpendicular to the field vector, the cosine of this angle would be 0; and if the cell moved directly toward the anode, the cosine of this angle would be −1. Dead cells (macrophages killed by *Salmonella*) or cells unresponsive to the EF (due to neuraminidase treatment) were either washed away or excluded from quantification by migration speed thresholding. The thresholds were estimated from fixed cells recorded in the same optical parameters and experiment setting for the live macrophages. The galvanotaxis assays and quantification of directionality and velocity in bone marrow-derived macrophages infected with Δ*nanH* and their isogenic wild type *Salmonella* were assigned in a double-blinded manner. Box-and-Whisker plots were generated using a custom R script (available upon request).

To simulate cell migration, each cell was numbered, and its x and y coordinates were measured on the first image and on every subsequent image in the image stack, with the x axis parallel to the applied electric field. The (x, y) data of each cell was imported with the ImageJ chemotaxis tool plugin and recalculated based on the optical parameters (lens and camera). Trajectories of the cells in each group were simulated in a Cartesian coordinate system by placing the first coordinates of each cell in the origin (0, 0).

To plot the polarized histograms, we combined θ of each time interval of tracked cells in each group. The vector θ, expressed in radians, were calculated from the coordinates of each trajectory. The distribution of θ in 12 angle bins and their abundance in percentage were plotted in Matlab (Mathworks) using a custom script (available upon request).

Measuring zeta potential. Macrophages were seeded onto 24-well tissue culture plates and infected with wild type *Salmonella* or Δ*nanH* following procedures as described above. Cells were fixed in 2% paraformaldehyde and washed with motility buffer (10^{-4} M potassium phosphate buffer at pH 7.0, with 10^{-4} M EDTA) (68). Cells were then gently collected by scraping with a "policeman" cell scraper, and subsequent measurements were done in motility buffer. Zeta potential was determined by electrophoretic light scattering at 25°C with a Zetasizer (Malvern Panalytical Ltd., Malvern, United Kingdom). Zeta potential was calculated in mV, and differences between groups were analyzed by Student's t test.

Flow cytometry. Wild type *Salmonella* or Δ*nanH*-infected macrophages according to the procedures described above, were incubated with Fc-block (BD, Franklin Lakes, NJ) on ice for 15 min, stained with biotinylated MAL-2, followed by fluorescein conjugated Streptavidin (Vector Laboratories, Inc. Burlingame, CA) for 1 h in each step on ice, and then stained with Aqua-LIVE/DEAD (Invitrogen, Carlsbad, CA) for 30 min at room temperature. Cells were washed after each step and before being analyzed on a BD Fortessa flow cytometer as described previously (29). Data were analyzed using FlowJo software (Tree Star Inc. Ashland, OR).

Lectin staining and confocal microscopy. Macrophages were seeded in custom-made EF chambers and treated/challenged by following procedures as described above. The cells were fixed with 4% paraformaldehyde immediately after EF exposure for 3 h with field orientation marked, stained with Biotinylated MAL-2, followed by fluorescein conjugated Streptavidin (Vector Laboratories, Inc. Burlingame, CA). Nuclei were labeled by Hoechst 33342. Cells were photographed using either an inverted (for cells on cover glass with no EF) or an upright (for cells on plastic EF chambers) Leica TCS SP8 confocal microscope (Leica microsystem). Images were processed using ImageJ. Beads and cells were counted using particle analysis function.

Statistics. Galvanotaxis data from representatives of at least four independent experiments were routinely presented as mean ± standard error (SE), unless stated otherwise. Distributions of macrophage polarity between control and neuraminidase treated were analyzed using χ^2 test. Student's t test and one-way ANOVA analysis followed by *post hoc* Tukey HSD test were used for paired or unpaired comparisons among two groups or multiple groups (more than two), respectively. ns: nonsignificant, *, $P < 0.05$, **, $P < 0.01$.

SUPPLEMENTAL MATERIAL

Supplemental material is available online only.

SUPPLEMENTAL FILE 1, PDF file, 0.2 MB.

SUPPLEMENTAL FILE 2, AVI file, 2.1 MB.

SUPPLEMENTAL FILE 3, XLSX file, 0.5 MB.

ACKNOWLEDGMENTS

Y. S. thanks Alex Mogilner for his initially financial support. We are deeply grateful to R. M. Tsolis and A. J. Bäumler for providing the *Salmonella* strains.

All raw data used to produce the figures are included in spreadsheets as supplemental materials. Matlab codes generated in this work are available on request.

This work was supported by the Defense Advanced Research Projects Agency (DARPA) HR001119S0027 to M. Z. (Program PI: Marco Rolandi), by NIH 1R21AI156409-01 to Y. S. and M. Z., and by interdepartment seed grant S-MPIDRGR from UC Davis School of Medicine to M. Z., Renee M. Tsolis, and Y. S. Funding from an early career award from the Burroughs Welcome Fund and by NIH 1DP2OD008752 supported E. M. The funders had no role in study design, data collection and analysis, decision to publish, or preparation of the manuscript.

The authors have declared that no competing interests exist.

REFERENCES

1. Mowat AM. 2003. Anatomical basis of tolerance and immunity to intestinal antigens. Nat Rev Immunol 3:331–341. https://doi.org/10.1038/nri1057.
2. Jones BD, Ghori N, Falkow S. 1994. Salmonella typhimurium initiates murine infection by penetrating and destroying the specialized epithelial M cells of the Peyer's patches. J Exp Med 180:15–23. https://doi.org/10.1084/jem.180.1.15.
3. Ohl ME, Miller SI. 2001. Salmonella: a model for bacterial pathogenesis. Annu Rev Med 52:259–274. https://doi.org/10.1146/annurev.med.52.1.259.
4. Shi C, Pamer EG. 2011. Monocyte recruitment during infection and inflammation. Nat Rev Immunol 11:762–774. https://doi.org/10.1038/nri3070.
5. Serbina NV, Jia T, Hohl TM, Pamer EG. 2008. Monocyte-mediated defense against microbial pathogens. Annu Rev Immunol 26:421–452. https://doi.org/10.1146/annurev.immunol.26.021607.090326.
6. Servant G, Weiner OD, Herzmark P, Balla T, Sedat JW, Bourne HR. 2000. Polarization of chemoattractant receptor signaling during neutrophil chemotaxis. Science 287:1037–1040. https://doi.org/10.1126/science.287.5455.1037.
7. Devreotes PN, Zigmond SH. 1988. Chemotaxis in eukaryotic cells: a focus on leukocytes and Dictyostelium. Annu Rev Cell Biol 4:649–686. https://doi.org/10.1146/annurev.cb.04.110188.003245.
8. Hensel M, Shea JE, Gleeson C, Jones MD, Dalton E, Holden DW. 1995. Simultaneous identification of bacterial virulence genes by negative selection. Science 269:400–403. https://doi.org/10.1126/science.7618105.
9. Ochman H, Soncini FC, Solomon F, Groisman EA. 1996. Identification of a pathogenicity island required for Salmonella survival in host cells. Proc Natl Acad Sci USA 93:7800–7804. https://doi.org/10.1073/pnas.93.15.7800.
10. Galan JE. 2001. Salmonella interactions with host cells: type III secretion at work. Annu Rev Cell Dev Biol 17:53–86. https://doi.org/10.1146/annurev.cellbio.17.1.53.
11. Galan JE, Curtiss R, 3rd. 1989. Cloning and molecular characterization of genes whose products allow Salmonella typhimurium to penetrate tissue culture cells. Proc Natl Acad Sci USA 86:6383–6387. https://doi.org/10.1073/pnas.86.16.6383.
12. Figueira R, Watson KG, Holden DW, Helaine S. 2013. Identification of salmonella pathogenicity island-2 type III secretion system effectors involved in intramacrophage replication of S. enterica serovar typhimurium: implications for rational vaccine design. mBio 4:e00065.
13. Celli J. 2006. Surviving inside a macrophage: the many ways of Brucella. Res Microbiol 157:93–98. https://doi.org/10.1016/j.resmic.2005.10.002.
14. Chaurasiya SK, Srivastava KK. 2009. Downregulation of protein kinase C-alpha enhances intracellular survival of Mycobacteria: role of PknG. BMC Microbiol 9:271. https://doi.org/10.1186/1471-2180-9-271.
15. Isberg RR, O'Connor TJ, Heidtman M. 2009. The Legionella pneumophila replication vacuole: making a cosy niche inside host cells. Nat Rev Microbiol 7:13–24. https://doi.org/10.1038/nrmicro1967.
16. Monack DM, Mecsas J, Ghori N, Falkow S. 1997. Yersinia signals macrophages to undergo apoptosis and YopJ is necessary for this cell death. Proc Natl Acad Sci USA 94:10385–10390. https://doi.org/10.1073/pnas.94.19.10385.
17. Vazquez-Torres A, Jones-Carson J, Bäumler AJ, Falkow S, Valdivia R, Brown W, Le M, Berggren R, Parks WT, Fang FC. 1999. Extraintestinal dissemination of Salmonella by CD18-expressing phagocytes. Nature 401:804–808. https://doi.org/10.1038/44593.
18. Pagan AJ, Ramakrishnan L. 2015. Immunity and immunopathology in the tuberculous granuloma. Cold Spring Harb Perspect Med 5:a018499. https://doi.org/10.1101/cshperspect.a018499.
19. Helaine S, Cheverton AM, Watson KG, Faure LM, Matthews SA, Holden DW. 2014. Internalization of Salmonella by macrophages induces formation of nonreplicating persisters. Science 343:204–208. https://doi.org/10.1126/science.1244705.
20. Shi R, Borgens RB. 1994. Embryonic neuroepithelial sodium-transport, the resulting physiological potential, and cranial development. Dev Biol 165:105–116. https://doi.org/10.1006/dbio.1994.1238.
21. McCaig CD, Rajnicek AM, Song B, Zhao M. 2005. Controlling cell behavior electrically: current views and future potential. Physiol Rev 85:943–978. https://doi.org/10.1152/physrev.00020.2004.
22. Levin M, Pezzulo G, Finkelstein JM. 2017. Endogenous bioelectric signaling networks: exploiting voltage gradients for control of growth and form. Annu Rev Biomed Eng 19:353–387. https://doi.org/10.1146/annurev-bioeng-071114-040647.
23. Levin M, Martyniuk CJ. 2018. The bioelectric code: an ancient computational medium for dynamic control of growth and form. Biosystems 164:76–93. https://doi.org/10.1016/j.biosystems.2017.08.009.
24. Barker AT, Jaffe LF, Vanable JW. 1982. The glabrous epidermis of cavies contains a powerful battery. Am J Physiol 242:R358–R366.
25. Zhao M, Song B, Pu J, Wada T, Reid B, Tai G, Wang F, Guo A, Walczysko P, Gu Y, Sasaki T, Suzuki A, Forrester JV, Bourne HR, Devreotes PN, McCaig CD, Penninger JM. 2006. Electrical signals control wound healing through phosphatidylinositol-3-OH kinase-gamma and PTEN. Nature 442:457–460. https://doi.org/10.1038/nature04925.
26. Nuccitelli R. 2003. A role for endogenous electric fields in wound healing. Curr Top Dev Biol 58:1–26. https://doi.org/10.1016/S0070-2153(03)58001-2.
27. Pai VP, Lemire JM, Paré J-F, Lin G, Chen Y, Levin M. 2015. Endogenous gradients of resting potential instructively pattern embryonic neural tissue via Notch signaling and regulation of proliferation. J Neurosci 35:4366–4385. https://doi.org/10.1523/JNEUROSCI.1877-14.2015.
28. Ferreira F, Luxardi G, Reid B, Zhao M. 2016. Early bioelectric activities mediate redox-modulated regeneration. Development 143:4582–4594.
29. Sun Y, Reid B, Ferreira F, Luxardi G, Ma L, Lokken KL, Zhu K, Xu G, Sun Y, Ryzhuk V, Guo BP, Lebrilla CB, Maverakis E, Mogilner A, Zhao M. 2019. Infection-generated electric field in gut epithelium drives bidirectional migration of macrophages. PLoS Biol 17:e3000044. https://doi.org/10.1371/journal.pbio.3000044.
30. Hoyer LL, Hamilton AC, Steenbergen SM, Vimr ER. 1992. Cloning, sequencing and distribution of the Salmonella typhimurium LT2 sialidase gene, nanH, provides evidence for interspecies gene transfer. Mol Microbiol 6:873–884. https://doi.org/10.1111/j.1365-2958.1992.tb01538.x.
31. Arabyan N, Park D, Foutouhi S, Weis AM, Huang BC, Williams CC, Desai P, Shah J, Jeannotte R, Kong N, Lebrilla CB, Weimer BC. 2016. salmonella degrades the host glycocalyx leading to altered infection and glycan remodeling. Sci Rep 6:29525. https://doi.org/10.1038/srep29525.
32. Liu CK, Wei G, Atwood WJ. 1998. Infection of glial cells by the human polyomavirus JC is mediated by an N-linked glycoprotein containing terminal alpha (2–6)-linked sialic acids. J Virol 72:4643–4649. https://doi.org/10.1128/JVI.72.6.4643-4649.1998.
33. Datsenko KA, Wanner BL. 2000. One-step inactivation of chromosomal genes in Escherichia coli K-12 using PCR products. Proc Natl Acad Sci USA 97:6640–6645. https://doi.org/10.1073/pnas.120163297.
34. Sun Y-H, Rolán HG, den Hartigh AB, Sondervan D, Tsolis RM. 2005. Brucella abortus virB12 is expressed during infection but is not an essential component of the type IV secretion system. Infect Immun 73:6048–6054. https://doi.org/10.1128/IAI.73.9.6048-6054.2005.
35. Auerbuch V, Lenz LL, Portnoy DA. 2001. Development of a competitive index assay to evaluate the virulence of Listeria monocytogenes actA mutants during primary and secondary infection of mice. Infect Immun 69:5953–5957. https://doi.org/10.1128/IAI.69.9.5953-5957.2001.
36. Nagura H, Asai J, Katsumata Y, Kojima K. 1973. Role of electric surface charge of cell membrane in phagocytosis. Acta Pathol Jpn 23:279–290.

37. Maverakis E, Kim K, Shimoda M, Gershwin ME, Patel F, Wilken R, Raychaudhuri S, Ruhaak LR, Lebrilla CB. 2015. Glycans in the immune system and the altered glycan theory of autoimmunity: a critical review. J Autoimmun 57:1–13. https://doi.org/10.1016/j.jaut.2014.12.002.
38. Knop J, Ax W, Sedlacek HH, Seiler FR. 1978. Effect of Vibrio cholerae neuraminidase on the phagocytosis of E. coli by macrophages in vivo and in vitro. Immunology 34:555–563.
39. Hoare JI. 2015. Electric fields are novel determinants of human macrophage functions. J Leukoc Biol.
40. Finkelstein EI, Chao P-h. G, Hung CT, Bulinski JC. 2007. Electric field-induced polarization of charged cell surface proteins does not determine the direction of galvanotaxis. Cell Motil Cytoskeleton 64:833–846. https://doi.org/10.1002/cm.20227.
41. Sun Y, Do H, Gao J, Zhao R, Zhao M, Mogilner A. 2013. Keratocyte fragments and cells utilize competing pathways to move in opposite directions in an electric field. Curr Biol 23:569–574. https://doi.org/10.1016/j.cub.2013.02.026.
42. Crennell SJ, Garman EF, Laver WG, Vimr ER, Taylor GL. 1993. Crystal-structure of a bacterial sialidase (from Salmonella-typhimurium Lt2) shows the same fold as an influenza-virus neuraminidase. Proc Natl Acad Sci USA 90: 9852–9856. https://doi.org/10.1073/pnas.90.21.9852.
43. Canard B, Cole ST. 1989. Genome organization of the anaerobic pathogen Clostridium perfringens. Proc Natl Acad Sci USA 86:6676–6680. https://doi.org/10.1073/pnas.86.17.6676.
44. Jermyn WS, Boyd EF. 2002. Characterization of a novel Vibrio pathogenicity island (VPI-2) encoding neuraminidase (nanH) among toxigenic Vibrio cholerae isolates. Microbiology (Reading) 148:3681–3693. https://doi.org/10.1099/00221287-148-11-3681.
45. Figueroa-Bossi N, Uzzau S, Maloriol D, Bossi L. 2001. Variable assortment of prophages provides a transferable repertoire of pathogenic determinants in Salmonella. Mol Microbiol 39:260–271. https://doi.org/10.1046/j.1365-2958.2001.02234.x.
46. Brüssow H, Canchaya C, Hardt W-D. 2004. Phages and the evolution of bacterial pathogens: from genomic rearrangements to lysogenic conversion. Microbiol Mol Biol Rev 68:560–602. https://doi.org/10.1128/MMBR.68.3.560-602.2004.
47. Taylor G, Vimr E, Garman E, Laver G. 1992. Purification, crystallization and preliminary crystallographic study of neuraminidase from Vibrio cholerae and Salmonella typhimurium LT2. J Mol Biol 226:1287–1290. https://doi.org/10.1016/0022-2836(92)91069-2.
48. Minami A, Ishibashi S, Ikeda K, Ishitsubo E, Hori T, Tokiwa H, Taguchi R, Ieno D, Otsubo T, Matsuda Y, Sai S, Inada M, Suzuki T. 2013. Catalytic preference of Salmonella typhimurium LT2 sialidase for N-acetylneuraminic acid residues over N-glycolylneuraminic acid residues. FEBS Open Bio 3: 231–236. https://doi.org/10.1016/j.fob.2013.05.002.
49. Vimr ER. 1994. Microbial sialidases: does bigger always mean better? Trends Microbiol 2:271–277. https://doi.org/10.1016/0966-842X(94)90003-5.
50. Garcia-Contreras R. 2012. Why in vivo may not equal in vitro - new effectors revealed by measurement of enzymatic activities under the same in vivo-like assay conditions. FEBS J 279:4145–4159. https://doi.org/10.1111/febs.12007.
51. Miao EA, Scherer CA, Tsolis RM, Kingsley RA, Adams LG, Bäumler AJ, Miller SI. 1999. Salmonella typhimurium leucine-rich repeat proteins are targeted to the SPI1 and SPI2 type III secretion systems. Mol Microbiol 34:850–864. https://doi.org/10.1046/j.1365-2958.1999.01651.x.
52. Miao EA, Brittnacher M, Haraga A, Jeng RL, Welch MD, Miller SI. 2003. Salmonella effectors translocated across the vacuolar membrane interact with the actin cytoskeleton. Mol Microbiol 48:401–415. https://doi.org/10.1046/j.1365-2958.2003.t01-1-03456.x.
53. McLaughlin LM, Govoni GR, Gerke C, Gopinath S, Peng K, Laidlaw G, Chien Y-H, Jeong H-W, Li Z, Brown MD, Sacks DB, Monack D. 2009. The Salmonella SPI2 effector SseI mediates long-term systemic infection by modulating host cell migration. PLoS Pathog 5:e1000671. https://doi.org/10.1371/journal.ppat.1000671.
54. Lombard V, Golaconda Ramulu H, Drula E, Coutinho PM, Henrissat B. 2014. The carbohydrate-active enzymes database (CAZy) in 2013. Nucleic Acids Res 42:D490–D495. https://doi.org/10.1093/nar/gkt1178.
55. Weber AN, Morse MA, Gay NJ. 2004. Four N-linked glycosylation sites in human toll-like receptor 2 cooperate to direct efficient biosynthesis and secretion. J Biol Chem 279:34589–34594. https://doi.org/10.1074/jbc.M403830200.
56. da Silva Correia J, Ulevitch RJ. 2002. MD-2 and TLR4 N-linked glycosylations are important for a functional lipopolysaccharide receptor. J Biol Chem 277: 1845–1854. https://doi.org/10.1074/jbc.M109910200.
57. Wang D, Ozhegov E, Wang L, Zhou A, Nie H, Li Y, Sun X-L. 2016. Sialylation and desialylation dynamics of monocytes upon differentiation and polarization to macrophages. Glycoconj J 33:725–733. https://doi.org/10.1007/s10719-016-9664-4.
58. Lokken KL, Walker GT, Tsolis RM. 2016. Disseminated infections with antibiotic-resistant non-typhoidal Salmonella strains: contributions of host and pathogen factors. Pathog Dis 74. https://doi.org/10.1093/femspd/ftw103.
59. Zhang X, Goncalves R, Mosser DM. 2008. The isolation and characterization of murine macrophages. Curr Protoc Immunol 14:1.
60. Sun Y-H, den Hartigh AB, Santos RL, Adams LG, Tsolis RM. 2002. virB-Mediated survival of Brucella abortus in mice and macrophages is independent of a functional inducible nitric oxide synthase or NADPH oxidase in macrophages. Infect Immun 70:4826–4832. https://doi.org/10.1128/IAI.70.9.4826-4832.2002.
61. Nakajima K-I, Zhu K, Sun Y-H, Hegyi B, Zeng Q, Murphy CJ, Small JV, Chen-Izu Y, Izumiya Y, Penninger JM, Zhao M. 2015. KCNJ15/Kir4.2 couples with polyamines to sense weak extracellular electric fields in galvanotaxis. Nat Commun 6:8532. https://doi.org/10.1038/ncomms9532.
62. Cohen DJ, Nelson WJ, Maharbiz MM. 2014. Galvanotactic control of collective cell migration in epithelial monolayers. Nat Mater 13:409–417. https://doi.org/10.1038/nmat3891.
63. Zhao M, Agius-Fernandez A, Forrester JV, McCaig CD. 1996. Orientation and directed migration of cultured corneal epithelial cells in small electric fields are serum dependent. J Cell Sci 109:1405–1414. https://doi.org/10.1242/jcs.109.6.1405.
64. Song B, Gu Y, Pu J, Reid B, Zhao Z, Zhao M. 2007. Application of direct current electric fields to cells and tissues in vitro and modulation of wound electric field in vivo. Nat Protoc 2:1479–1489. https://doi.org/10.1038/nprot.2007.205.
65. Sun YH. 2011. Airway epithelial wounds in rhesus monkey generate ionic currents that guide cell migration to promote healing. J Appl Physiol
66. Tai G, et al. 2009. Electrotaxis and wound healing: experimental methods to study electric fields as a directional signal for cell migration. Methods Mol Biol 571:77–97. https://doi.org/10.1007/978-1-60761-198-1_5.
67. Gruler H, Nuccitelli R. 1991. Neural crest cell galvanotaxis: new data and a novel approach to the analysis of both galvanotaxis and chemotaxis. Cell Motil Cytoskeleton 19:121–133. https://doi.org/10.1002/cm.970190207.
68. Adler J, Shi W. 1988. Galvanotaxis in bacteria. Cold Spring Harbor Symp Quant Biol 53 Pt 1:23–25. https://doi.org/10.1101/sqb.1988.053.01.006.
69. Stojiljkovic I, Baumler AJ, Heffron F. 1995. Ethanolamine utilization in Salmonella typhimurium: nucleotide sequence, protein expression, and mutational analysis of the cchA cchB eutE eutJ eutG eutH gene cluster. J Bacteriol 177:1357–1366. https://doi.org/10.1128/jb.177.5.1357-1366.1995.
70. Baumler AJ, et al. 1997. Synergistic effect of mutations in invA and lpfC on the ability of Salmonella typhimurium to cause murine typhoid. Infect Immun 65:2254–2259. https://doi.org/10.1128/iai.65.6.2254-2259.1997.
71. McClelland M, Sanderson KE, Spieth J, Clifton SW, Latreille P, Courtney L, Porwollik S, Ali J, Dante M, Du F, Hou S, Layman D, Leonard S, Nguyen C, Scott K, Holmes A, Grewal N, Mulvaney E, Ryan E, Sun H, Florea L, Miller W, Stoneking T, Nhan M, Waterston R, Wilson RK. 2001. Complete genome sequence of Salmonella enterica serovar Typhimurium LT2. Nature 413: 852–856. https://doi.org/10.1038/35101614.